NANO LETTERS

Letter

pubs.acs.org/NanoLett

Temperature-Gated Thermal Rectifier for Active Heat Flow Control

Jia Zhu,[†,∥] Kedar Hippalgaonkar,[†,∥] Sheng Shen,[†] Kevin Wang,[‡] Yohannes Abate,[§] Sangwook Lee,[‡] Junqiao Wu,[‡] Xiaobo Yin,[†] Arun Majumdar,*[,†] and Xiang Zhang*[,†]

[†]Department of Mechanical Engineering and [‡]Department of Materials Science and Engineering, University of California at Berkeley, Berkeley, California 94720, United States

[§]Department of Physics and Astronomy, Georgia State University, Atlanta, Georgia 30303, United States

Supporting Information

ABSTRACT: Active heat flow control is essential for broad applications of heating, cooling, and energy conversion. Like electronic devices developed for the control of electric power, it is very desirable to develop advanced all-thermal solid-state devices that actively control heat flow without consuming other forms of energy. Here we demonstrate temperature-gated thermal rectification using vanadium dioxide beams in which the environmental temperature actively modulates asymmetric heat flow. In this three terminal device, there are two switchable states, which can be regulated by global heating. In the "Rectifier" state, we observe up to 28% thermal rectification. In the "Resistor" state, the thermal rectification is significantly suppressed (<1%). To the best of our knowledge, this is the first demonstration of solid-state active-thermal devices with a large rectification in the Rectifier state. This temperature-gated rectifier can have substantial implications ranging from autonomous thermal management of heating and cooling systems to efficient thermal energy conversion and storage.

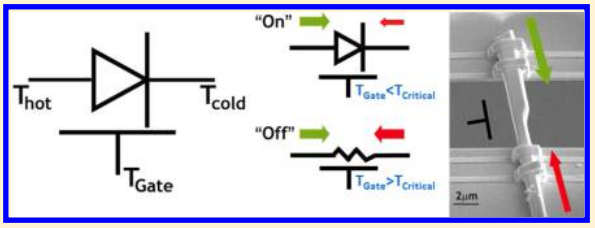

KEYWORDS: *Thermal rectification, nanoscale heat transport, vanadium dioxide, phonons*

Heat and charge transport in condensed matter were first characterized about two centuries ago by the well-known Fourier's[1] ($\vec{q} = -k\nabla\vec{T}$) and Ohm's[2] ($\vec{J} = -\sigma\vec{E}$) laws, respectively. The history of how the science of heat and charge transport has evolved, however, is very different. The progress in material processing (such as purification of semiconductors) and fundamental understanding (quantum mechanics) led to the invention of many electronic devices such as transistors to actively control and manipulate charge transport. Such devices have been widely deployed and have touched almost all aspects of modern life in what we now call the information revolution. In stark contrast, heat transport in condensed matter has remained in the realm of the Fourier law and its manipulation beyond has been largely absent. Yet, about 90% of the world's energy utilization occurs through heating and cooling, making it one of the most critical aspects of any modern economy.[3] Hence, the ability to actively manipulate heat transport in ways akin to that for charge transport could potentially significantly impact utilization of energy resources.

A few theoretical proposals have been made envisioning control of heat flow in solid-state devices[4,5] and electrically tuned solid-state thermal memory has recently been experimentally realized.[6] Most development has explored the possibility of thermal rectification[7,8] in which the system thermal conductance depends on the direction of thermal gradient. The level of thermal rectification is commonly[7] defined as the following

$$R = \frac{G_H - G_L}{G_L}$$

Here G_H and G_L are the thermal conductances of the sample in the directions of higher and lower heat flows under the same temperature difference, respectively. Several approaches have been theorized for achieving thermal rectification, such as using materials with opposite trends in thermal conductivity as a function of temperature[9,10] or asymmetrical phonon density of states in graphene nanoribbons.[11] The rapid advancement of nanofabrication has enabled the synthesis of nanostructures with a variety of materials for both novel applications[12−16] and to explore condensed matter science.[17] Specifically, individual carbon or boron nitride nanotubes with asymmetric mass loading were reported to have thermal rectification of about 2−7%.[7] However, a pure active thermal device where heat as an input can modulate thermal transport has never been realized.

In condensed matter, both phonons and electrons carry heat. Metals are generally good conductors of heat through electrons. Manipulating heat in nonmetals requires tuning of quantized lattice vibrations or phonons. Heat transfer with a single energy carrier (either electrons and phonons) has been studied in detail in many condensed matter systems. Can the interplay between the two energy carriers at metal−insulator interfaces potentially lead to an asymmetry when the direction of heat flow is reversed? Very early work in a CuO−Cu system showed

Received: June 17, 2014
Published: July 10, 2014

   dx.doi.org/10.1021/nl502261m | *Nano Lett.* 2014, 14, 4867−4872

thermal rectification due to a single metal−insulator interface.[18] Here we demonstrate the first temperature-gated thermal rectifier devices using VO_2 beams. Interestingly, thermal rectification in the beams can be actively switched on and off by changing the device temperature, which controls the metallic and insulating phases, thus functioning as a thermal gate. Maximum rectification of 28% is observed below 340 K when mixed metallic and insulating phases coexist in the VO_2 beam. Once the devices are heated above 340 K and they become completely metallic, they behave as ordinary thermal resistors, where thermal rectification is switched off (<1%) (see Figure 1A for a depiction of the device functionality).

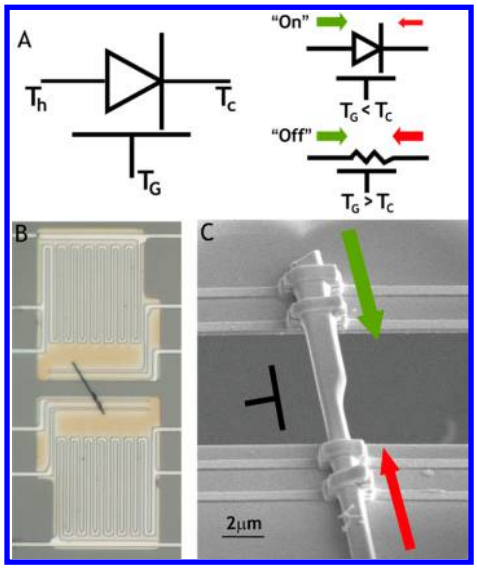

Figure 1. (A) Symbolic diagram of temperature-gated thermal rectifier. In the "Rectification" or "on" state, thermal flow depends on the direction of applied thermal gradient, representing thermal rectification. In the "Resistor" or "off" state, thermal flow does not depend on the sign of thermal gradient, essentially the behavior of a resistor. The on/off state can be controlled by T_G. (B) Optical microscope image of an asymmetrical VO_2 beam on suspended membranes for thermal conductance measurement. (C) Scanning electron microscopy (SEM) image of an asymmetrical VO_2 beam. The VO_2 beams used in this study have a uniform thickness (typically 500 nm to 1 μm) with one end of narrow width (300−900 nm) and the other end of wide width (600 nm to 2 μm). The heat flow through the beam (Q) in either direction denoted by the arrows is accurately measured while the suspended platforms are maintained as isotherms at hot and cold temperatures, T_h and T_c, respectively (details in Supporting Information).

Our material system of choice for this study is the family of vanadium oxides. Single crystalline VO_2 beams have been investigated extensively as a unique material system for studying the complexity of metallic and insulating phases that can be induced by temperature, strain, stoichiometry and light.[19−23] Thin films of polycrystalline VO_2 have shown that the insulator-to-metal transition occurs at the transition temperature ~340 K via nucleation of isolated nanoscale puddles of metallic phases in a background of the insulator phase, which then grow and merge as the transition progresses.[24] The thermal conductivity of polycrystalline stoichiometric VO_2 films was also studied close to ~340 K and increased by as much as 60% due to the phase transition.[25]

We synthesized VO_2 beams using a modified vapor transport method (Supporting Information Methods) and studied their electrical properties.[26] The structure and electrical properties confirm a VO_2 backbone. From the synthesized beams, we specifically selected beams that are tapered in shape (similar to the beam illustrated in Figure 1B,C), expecting local stresses and stoichiometry changes that could enable the coexistence of metallic and insulating phases coexisting in the beam.[19] Such a 5−10 μm long tapered beam is then transferred to a silicon microdevice so as to form a bridge between two parallel, suspended SiN_X membranes, each consisting of microfabricated symmetric resistive platinum coils, for thermal and electrical transport measurements[27] (Figure 1B). The platinum coils are used as both heaters and resistive thermometers (Supporting Information Methods). To make electrical and thermal contact, a platinum/carbon composite was deposited symmetrically on both ends using a focused ion beam. Therefore, both thermal and electrical conductance can be measured for the device. A resistive heater is used to heat the whole chip uniformly inside a cryostat to control the global device temperature, T_G. The measurement is performed in a cryostat at ~2 μTorr to prevent conduction and convection losses. (Supporting Information 2).

Figure 2A shows measured heat flow, Q, and the temperature difference, ΔT, across a tapered beam at T_G =320 K below the VO_2 insulator−metal phase transition temperature of 340 K. The heat flow, Q, increases linearly with ΔT (<1 K). However, the thermal conductance, $G = Q/\Delta T$, or the slope, differs depending on the direction of heat flow. The thermal conductance of the tapered beam when heat is flowing from the narrow to the broader side (62.2 ± 0.5 nW/K) is significantly smaller than that in the other direction (80.1 ± 0.6 nW/K). This represents a 28 ± 1.4% thermal rectification, which is the highest ever reported to the best of our knowledge. Also shown in Figure 2B is δQ, which is the deviation of the heat flow in one direction, Q, from the extrapolated linear curve representing the conductance in the opposite direction. Figure 2C,D shows similar plots for the same VO_2 beam at T_G = 385 K, which is higher than the phase transition temperature where the VO_2 beam is fully metallic. In contrast to Figure 2A,B, it is clear that no rectification is observed and the thermal conductance in both directions increases to 94 ± 0.4 nW/K. The same plots of Q and δQ at 320 K of a uniform or untapered VO_2 beam show that there is no rectification (Supporting Information 3a).

The maximum thermal rectification of six tapered VO_2 beams are tabulated in Table 1 for T_G < 340 K. The values range from 10 to 20% for different beams and T_G is different for different beams. Rectification is turned off to below 1% for T_G > 340 K. Note that in beam V, the rectification persists above the insulator-to-metal transition for stoichiometric VO_2. We ascribe this to an excess of oxygen, thus shifting the electronic transition temperature to much higher temperatures. As control experiments, symmetric beams with uniform width, which have no variation in stoichiometry, are also measured and no apparent thermal rectification effects are observed (<3%) at all temperatures below and above the transition temperature of 340 K (Supporting Information 3b).

Figure 3A shows the thermal conductance in the two directions (green and red) as a function of global temperature for a representative VO_2 beam. Between 250 and 340 K, the conductance is different in different directions, which is discussed in detail later. It is observed that the degree of rectification, R, (black closed circles) peaks at 320 K, lower than

dx.doi.org/10.1021/nl502261m | Nano Lett. 2014, 14, 4867−4872

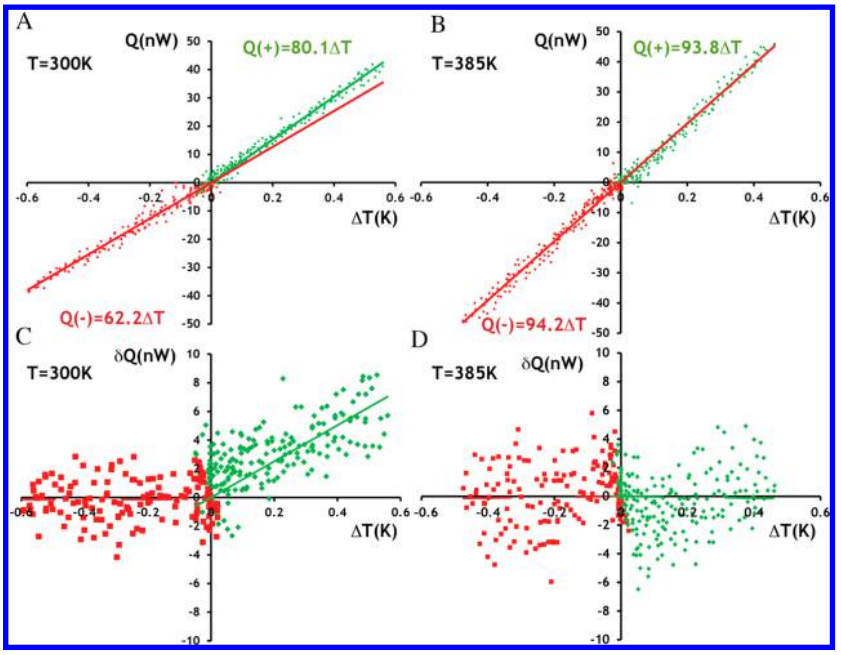

Figure 2. (A,C) Q as a function of ΔT across the VO_2 beams at 300 and 350 K, respectively. Different signs (+) and (−) of Q represent different directions of heat transfer. (B,D) Heat flow deviation (δQ) as a function of temperature difference across the VO_2 beams at 300 and 385 K, respectively.

Table 1. Thermal Conductance and Maximum Thermal Rectification (at T_G = 300−320 K) of six Different VO_2 Beams

	T_G < 340 K			T_G > 340 K		
no.	G+ (nW/K)	G− (nW/K)	R (%)	G+ (nW/K)	G− (nW/K)	R (%)
I	80.1 ± 0.6	62.2 ± 0.5	28.8 ± 1.4%	93.8 ± 0.4	94.2 ± 0.4	−0.5 ± 0.6%
II	144 ± 2.1	123 ± 1.6	16.9 ± 2.0%	165 ± 2.7	167 ± 3.0	1.0 ± 2.4%
III	113 ± 0.3	103 ± 0.3	9.1 ± 0.4%	119 ± 0.4	117 ± 0.3	1.1 ± 0.4%
IV	191 ± 0.8	171 ± 0.6	12.1 ± 0.6%	181 ± 0.6	181 ± 0.6	0.0 ± 0.5%
V	58.5 ± 0.1	55.3 ± 0.1	5.9 ± 0.2	58.6 ± 0.1	56.8 ± 0.1	3.2 ± 0.2
VI	181 ± 0.5	169 ± 0.6	7.2 ± 0.5%	186 ± 0.5	184 ± 0.6	0.9 ± 0.5%

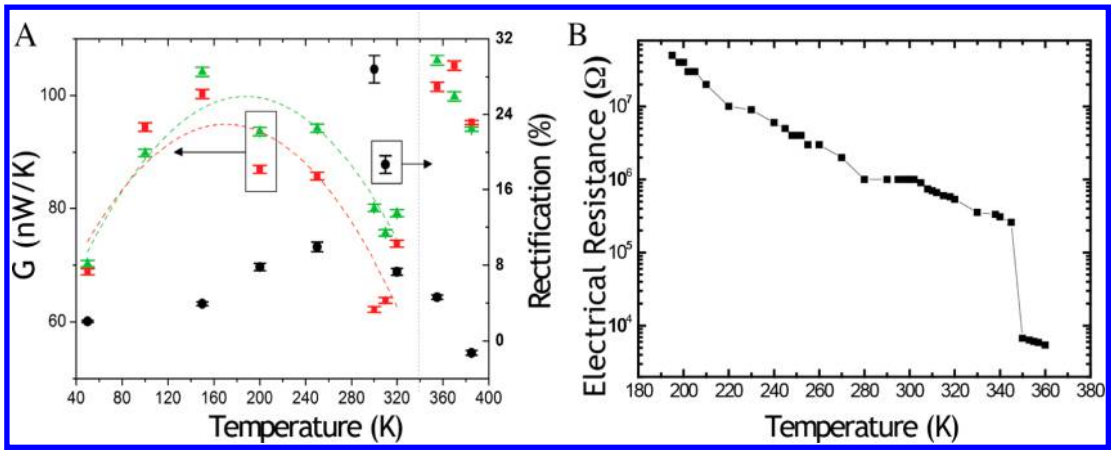

Figure 3. (A) Thermal conductance of an asymmetrical VO_2 beam as a function of global temperatures along two opposite directions (green triangles and red squares). The thermal conductance is found to be measurably higher when heat flows from the wide end to the narrow end. At low temperatures, the rectification (black closed circles) disappears and the conductance from either end is identical; this is expected as the whole wire is in the insulating phase and should behave as a normal dielectric. (B) The electrical resistance of VO_2 beam as a function of global temperature. The resistance could not be measured below 180 K due to saturation. The arrows in Figure 1 denote the direction of heat flow in which high (green) and low (red) thermal conductance was observed.

the phase transition of 340 K and decreases as the temperature is increased or decreased away from the transition. Above the VO_2 insulator−metal transition temperature (~340 K), the electronic density of states at the Fermi level increase significantly and electrons start contributing to the thermal conductance, which explains a sudden increase. This is also consistent with electrical resistance measurements (see Figure 3B), which show a drop in magnitude by two orders at 340 K

dx.doi.org/10.1021/nl502261m | Nano Lett. 2014, 14, 4867−4872

indicating the characteristic insulator-to-metal phase transition, consistent with reports in literature for the electronic VO_2 phase transition.[22] Below 135 K, the electronic contribution is negligible and phonons dominate heat conduction. In this temperature range, we do not observe any rectification as well. The phonon mean free path is limited by scattering from either defects, interfaces, or boundaries, and the thermal conductance increases with temperature due to increase in phonon population. Temperature-dependent conductance and rectification plots similar to Figure 3A for beam II are shown in Supporting Information 4.

In order to understand the mechanism behind temperature-dependent rectification, we first consider the effect of the asymmetric geometry on the phonon mean free path. It has been proposed that an asymmetric geometry or roughness may cause thermal rectification in materials when phonons dominate heat conduction and the phonon mean free path is comparable to the characteristic length of the structure.[4] The average phonon mean free path can be estimated by kinetic theory: $\Lambda = (3k)/(cv_g)$. In the insulating phase at 300 K, $k \approx 6$ Wm^{-1} K^{-1} is the measured thermal conductivity of a representative VO_2 beam, the volumetric heat capacity $c = 3$ J cm^{-3} K^{-1} is taken to be the bulk value of VO_2,[28] and $v_g \approx v_s \approx 4000$ ms^{-1} is estimated from the acoustic speed of sound in the c-axis [001] direction,[29] thus $\Lambda \approx 1.5$ nm. In the metallic phase at 350 K, if we take $k \approx 6$ Wm^{-1} K^{-1}, $c = 3$ J cm^{-3} K^{-1} and $v_s \approx 4000$ ms^{-1}, then $\Lambda \approx 1.5$ nm. Note that our estimation of the phonon mean free path based on kinetic theory is an underestimation since (a) the average phonon group velocity is smaller than the speed of sound, which arises from the acoustic modes. Especially accounting for multiple atoms in the primitive cell of VO_2, the optical modes can contribute significantly to the thermal conductivity, and (b) phonon scattering is highly frequency dependent, and here we estimate using only the gray model, which ascribes a frequency-independent mean free path. However, considering that the lateral length scale of our beams is ~1000 times higher than the estimated mean free path, thermal rectification due to a geometric effect that requires boundary scattering to be dominant is very unlikely. In addition, below 50 K the phonon mean free path should increase by about 1 order of magnitude. Therefore, any thermal rectification caused by asymmetrical geometry should be a lot more significant at lower temperature, which is not observed in Figure 3A. So it is not possible that uneven phonon heat conduction due to asymmetrical geometry could cause the observed large thermal rectification. This further indicates that the macroscopic geometric ratio between the broad and narrow widths of the beam across the taper is not expected to scale with the observed thermal rectification.

Next, we explore if the insulator-to-metal phase transition in VO_2 can be responsible for thermal rectification. A recent theoretical study estimated the thermal interface resistance (TIR) on the metallic side between a metal and an insulator by employing the two-temperature model to account for the lack of equilibrium between electrons and phonons near a metal−insulator interface.[30] This model only considers the TIR due to the electron−phonon cooling rate, G_{e-l}. The phonon−electron cooling rate, G_{l-e} can be different, leading to an asymmetry close to the interface. This forms the basis for the theoretical prediction of thermal rectification if metallic and insulating phases coexist in a material system.[8] Further, due to nonlinearity and asymmetry in the electron−phonon interaction another prediction estimates rectification in a one-dimensional chain that depends on the coupling strength and the temperature gradient across the interface.[31] Thus, in order to observe significant thermal rectification in a metal−insulator system, first the thermal resistance due to electron−phonon scattering should dominate over the phonon−phonon coupling resistance. In the vanadium oxide system, a small ~1% lattice distortion[22] in the rutile and monoclinic phases should ensure good acoustic match to reduce thermal resistance from phonon−phonon coupling. Therefore, it is possible that the electron−phonon scattering may be dominant for the thermal resistance at metal−insulator interfaces in VO_2 beams. Second, an abundance of coexisting metallic and insulating phases with an inherent asymmetry must prevail in the beams. Previous work has shown the coexistence of metallic and insulating phases within a single beam during phase transition.[19,20,22]

Intriguingly, in our case thermal rectification was observed not only near phase transition temperature 340 K but also over large span of temperature ~100 K below, provoking the question as to the role of the taper of the VO_2 beams. Even though the VO_2 beams show characteristic electronic transition temperature (340 K) (Supporting Information 5), it has been known that vanadium oxide can form Magnéli phases with a deficiency of oxygen, given by the general formula V_nO_{2n-1}, or excess of oxygen described by V_nO_{2n+1}. These are crystallographic shear compounds with a rutile VO_2 backbone.[32] The role of stoichiometry in $V_nO_{2n-1} = V_2O_3 + (n-2)VO_2$, or $V_nO_{2n+1} = V_2O_5 + (n-2)VO_2$ single crystals has been studied in meticulous detail.[33] As observed in Figure 3A, the "on" state of rectification exists between 250 and 340 K, where the V_2O_3/V_2O_5 shear planes would be metallic and the VO_2 matrix would be insulating. Therefore, a small variation in stoichiometry of vanadium oxide can cause the existence of metal−insulator interfaces over a very large range of temperature.[33] This is suggested in Figure 3A, between 250 and 340 K where rectification exists, in the regime where thermal conductance decreases with increasing temperature. While phonon−phonon Umklapp scattering is one possible cause for this behavior, it can also be attributed to the appearance of interfaces created by the formation and coexistence of multiple phases of vanadium oxide that may be not electronically connected, nevertheless impeding phonons due to interface scattering.

The second critical requirement to observe rectification is an asymmetry in these mixed states. In order to directly image the mixed phases and their spatial organization, we employed a scattering type scanning near-field optical microscope (s-SNOM). s-SNOM allows direct imaging of the evolution of insulating and metallic phases with increasing temperature with high spatial resolution as demonstrated previously for microcrystals and polycrystalline films. A linearly polarized probing CO_2 laser (wavelength, $\lambda = 10.7$ μm) is focused on the tip−sample interface. High harmonic demodulation coupled with pseudoheterodyne interferometer are used to detect the near-field signal with ~30 nm spatial resolution above the tapered VO_2 beam.[24,34] The image contrast is determined by the local spatially varying dielectric function of the surface. Hence, regions of the metallic phase due to larger effective tip−sample polarizablility result in higher s-SNOM amplitude signal compared with that of the insulating phase (more details about the technique are discussed in Supporting Information 6). The wavelength of the laser was chosen specifically in order to maximize the difference in the optical conductivity of the insulating and metallic phases of VO_2 and thus achieve optimum s-SNOM amplitude contrast at different temper-

dx.doi.org/10.1021/nl502261m | Nano Lett. 2014, 14, 4867−4872

atures. Interestingly, for a tapered beam (AFM topography shown in Figure 4A,D) demonstrating ~15% thermal

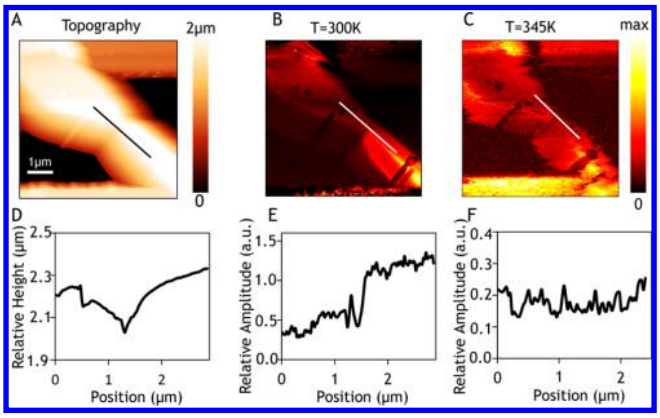

Figure 4. (A,D) AFM topography obtained via tapping mode on a suspended tapered VO_2 beam exhibiting 15% rectification at 300 K. The edges of the suspended membranes holding the beam are visible on the top and bottom of the image. A line profile is drawn across the tapered region on the beam with the relative height in μm illustrated in (D) as a function of beam length. (B) Near-field amplitude signal obtained at second harmonic demodulation at 300 K on the same tapered VO_2 beam. The black spots on the beam are dirt particles, possibly carbon, with a negligible dielectric value at the excitation frequency corresponding to a CO_2 laser wavelength of 10.7 μm. A white line profile is drawn across the taper with the corresponding line profile of the near field signal amplitude in (E). The near-field amplitude contrast changes significantly across the taper with the narrow region of the beam being more metallic and the broad section insulating. (C) The near field amplitude signal obtained on the same tapered VO_2 beam at 345 K, higher than the insulator–metal phase transition temperature of VO_2. The black spots, which are impurities on the surface, remain dark in contrast indicating temperature-independent contrast. A white line is drawn at the same location as that in (B) across the taper with its corresponding near field amplitude line profile illustrated in (F). The metal–insulator contrast difference seen in (E) at 300 K across the taper disappears at this higher temperature of 345 K, illustrating that the phase transition has occurred and that the phase is homogeneously metallic.

rectification at 300 K (data not shown in Table 1 as device broke before reaching 340 K during measurement), there exists s-SNOM amplitude contrast across the taper confirming phase coexistence at the same temperature (Figure 4B,E), which disappears when the sample is heated up to 345 K (Figure 4C,F). Note that the s-SNOM images show on average that the narrow side of the tapered VO_2 beam is metallic, while the broader side is insulating. Because the resolution is limited to ~30 nm, we did not observe any crystallographic shear planes with this technique. A similar experiment on a uniform cross-section beam shows no amplitude contrast evolution (Supporting Information 6).

While the s-SNOM figure (Figure 4B,C) shows unequivocally the presence of asymmetric mixed phases, the origin of these remains to be ascertained. As explained above, these could be due to a variation of stoichiometry along the beam length. We also found a signature of mixed vanadium oxide phases in tapered beams using auger electron spectroscopy (AES) (Supporting Information 7). In addition to stoichiometry, recent work shows that the phase transition also depends on stress fields within single VO_2 beams.[22] It is possible that the taper created during the beam growth may lead to stress gradients that could produce geometrical and size distributions of metallic and insulating domains and interfaces near the taper. These can amplify the rectification achieved by single interfaces. Similar distributions were previous reported by bending the beam.[19] Hence, while the insulator-to-metal phase transition is critical to thermal rectification, the taper and composition variation may also contribute to the effect by unique distributions of metal–insulator domains. On the basis of the interfacial thermal conductance from the two-temperature model described earlier,[30] we have estimated the approximate effective metal–insulator interface area required to observe the thermal rectification (details in Supporting Information 9).

The metal–insulator domains and interfaces can be rationally engineered to control the thermal transport. In stoichiometric VO_2 beams, an array of metal domains can be created below 340 K by either substitutional doping[35,36] or local stressing.[19,22] In addition, metal domains can be stabilized along these VO_2 beams at sub-340 K temperatures by encoding stoichiometry variation during the growth[21] or postgrowth hydrogenation.[37] Over the last several decades, while tremendous progress has been made in understanding the complexity of the phase transition in the family of vanadium oxides, the underlying physics still remains largely elusive.[38] Its impact on thermal transport is much less explored and has yet to be fully understood. Rational synthesis of vanadium oxide based beams with controlled local stresses and/or stoichiometry with a lack or excess of oxygen can open up pathways to further manipulate heat transfer in these systems.

In summary, we report a large thermal rectification up to 28% in VO_2 beams that is gated by the environmental temperature. It is the first demonstration of an active three-terminal thermal device exhibiting an "on" rectifying state over a large range of temperature (T_G = 250–340 K) and "off" resistor state (T_G < 250 K or T_G > 340 K). By changing temperature, one can switch the rectification, much like a gate voltage switches a thyristor between two states of electrical conductance. The realization of such unique thermal control is a consequence of the interplay between metallic and insulating phases due to the rich parameter space provided by the vanadium–oxygen material family. Such novel all-thermal devices may spurn interesting applications in autonomous thermal flow control and efficient energy harvesting.

■ ASSOCIATED CONTENT

Supporting Information

Details about synthesis of VO_2 nanowires, measurement, Auger Spectroscopy, additional data, and discussion and error analysis. This material is available free of charge via the Internet at http://pubs.acs.org.

■ AUTHOR INFORMATION

Corresponding Authors

*E-mail: (X.Z.) xiang@berkeley.edu.
*E-mail: (A.M.) 4majumdar@gmail.com.

Author Contributions

‖J.Z. and K.H. contributed equally.

Notes

The authors declare no competing financial interest.

■ ACKNOWLEDGMENTS

This work was supported by the U.S. Department of Energy, Basic Energy Sciences Energy Frontier Research Center (DoE-LMI-EFRC) under award DOE DE-AC02-05CH11231. This

materials synthesis part was supported by the U.S. Department of Energy Early Career Award DE-FG02-11ER46796. Y.A. acknowledges support from the U.S. Army Research Office, Agreement Number: W911NF-12-1-0076.

REFERENCES

(1) Fourier, J. B. J. *Théorie analytique de la chaleur*; Chez Firmin Didot Père et Fils: Paris, 1822.
(2) Ohm, G. S. *Die galvanische kette: mathematisch*; T. H. Riemann: Berlin, 1827.
(3) Chu, S.; Majumdar, A. *Nature* **2012**, *488*, 294−303.
(4) Li, B.; Wang, L.; Casati, G. *Phys. Rev. Lett.* **2004**, *93*, 1−4.
(5) Li, N.; Ren, J.; Wang, L.; Zhang, G.; Hänggi, P.; Li, B. *Rev. Mod. Phys.* **2012**, *84*, 1045−1066.
(6) Xie, R.; Bui, C. T.; Varghese, B.; Zhang, Q.; Sow, C. H.; Li, B.; Thong, J. T. L. *Adv. Funct. Mater.* **2011**, *21*, 1602−1607.
(7) Chang, C. W.; Okawa, D.; Majumdar, A.; Zettl, A. *Science* **2006**, *314*, 1121−1124.
(8) Roberts, N. A.; Walker, D. G. *Int. J. Therm. Sci.* **2011**, *50*, 648−662.
(9) Dames, C. *J. Heat Transfer* **2009**, *131*, 061301.
(10) Jezowski, A.; Rafalowicz, J. *Phys. Status Solidi* **1978**, *47*, 229−232.
(11) Yang, N.; Zhang, G.; Li, B. *Appl. Phys. Lett.* **2009**, *95*, 033107.
(12) Xia, Y.; Yang, P.; Sun, Y.; Wu, Y.; Mayers, B.; Gates, B.; Yin, Y.; Kim, F.; Yan, H. *Adv. Mater.* **2003**, *15*, 353−389.
(13) Cui, Y.; Wei, Q.; Park, H.; Lieber, C. M. *Science* **2001**, *293*, 1289−1292.
(14) Wang, Z. L.; Song, J. *Science* **2006**, *312*, 242−246.
(15) Hochbaum, A. I.; Chen, R.; Delgado, R. D.; Liang, W.; Garnett, E. C.; Najarian, M.; Majumdar, A.; Yang, P. *Nature* **2008**, *451*, 163−167.
(16) Boukai, A. I.; Bunimovich, Y.; Tahir-Kheli, J.; Yu, J.-K.; Goddard, W. a; Heath, J. R. *Nature* **2008**, *451*, 168−171.
(17) Xiang, J.; Vidan, A.; Tinkham, M.; Westervelt, R. M.; Lieber, C. M. *Nat. Nanotechnol.* **2006**, *1*, 208−213.
(18) Starr, C. *Physics (College. Park, MD)* **1936**, *7*, 15−19.
(19) Cao, J.; Ertekin, E.; Srinivasan, V.; Fan, W.; Huang, S.; Zheng, H.; Yim, J. W. L.; Khanal, D. R.; Ogletree, D. F.; Grossman, J. C.; Wu, J. *Nat. Nanotechnol.* **2009**, *4*, 732−737.
(20) Wei, J.; Wang, Z.; Chen, W.; Cobden, D. H. *Nat. Nanotechnol.* **2009**, *4*, 420−424.
(21) Zhang, S.; Chou, J. Y.; Lauhon, L. J. *Nano Lett.* **2009**, *9*, 4527−4532.
(22) Wu, J.; Gu, Q.; Guiton, B. S.; Leon, N. P.; De Ouyang, L.; Park, H. *Nano Lett.* **2006**, *6*, 2313−2317.
(23) Cavalleri, A.; Tóth, C.; Siders, C.; Squier, J.; Ráksi, F.; Forget, P.; Kieffer, J. *Phys. Rev. Lett.* **2001**, *87*, 1−4.
(24) Qazilbash, M. M.; Brehm, M.; Chae, B.-G.; Ho, P.-C.; Andreev, G. O.; Kim, B.-J.; Yun, S. J.; Balatsky, a V; Maple, M. B.; Keilmann, F.; Kim, H.-T.; Basov, D. N. *Science* **2007**, *318*, 1750−1753.
(25) Oh, D.-W.; Ko, C.; Ramanathan, S.; Cahill, D. G. *Appl. Phys. Lett.* **2010**, *96*, 151906.
(26) Kodambaka, S.; Tersoff, J.; Reuter, M. C.; Ross, F. M. *Science* **2007**, *316*, 729−732.
(27) Shi, L.; Li, D.; Yu, C.; Jang, W.; Kim, D.; Yao, Z.; Kim, P.; Majumdar, A. *J. Heat Transfer* **2003**, *125*, 881−888.
(28) Berglund, C.; Guggenheim, H. *Phys. Rev.* **1969**, *185*, 1022−1033.
(29) Maurer, D.; Leue, A.; Heichele, R.; Mu, V. *Phys. Rev. B* **1999**, *60*, 249−252.
(30) Majumdar, A.; Reddy, P. *Appl. Phys. Lett.* **2004**, *84* (23), 4768−4770.
(31) Zhang, L.; Lü, J.-T.; Wang, J.-S.; Li, B. *J. Phys.: Condens. Matter* **2013**, *25*, 445801.
(32) Wells, A. F. *Structural Inorganic Chemistry*; Oxford Classic Texts in the Physical Sciences; OUP: Oxford, 2012.
(33) Kachi, S.; Kosuge, K.; Okinaka, H. *J. Solid State Chem.* **1973**, *6*, 258−270.
(34) Jones, A. C.; Berweger, S.; Wei, J.; Cobden, D.; Raschke, M. B. *Nano Lett.* **2010**, *10*, 1574−1581.
(35) Lee, S.; Cheng, C.; Guo, H.; Hippalgaonkar, K.; Wang, K.; Suh, J.; Liu, K.; Wu, J. *J. Am. Chem. Soc.* **2013**, *135*, 4850−4855.
(36) Gu, Q.; Falk, A.; Wu, J.; Ouyang, L.; Park, H. *Nano Lett.* **2007**, *7*, 363−366.
(37) Wei, J.; Ji, H.; Guo, W.; Nevidomskyy, A. H.; Natelson, D. *Nat. Nanotechnol.* **2012**, *7*, 357−362.
(38) Tao, Z.; Han, T.-R.; Mahanti, S.; Duxbury, P.; Yuan, F.; Ruan, C.-Y.; Wang, K.; Wu, J. *Phys. Rev. Lett.* **2012**, *109*, 1−5.